Distinct respone of Northern Hemisphere land monsoon precipitation to transient and stablized warming scenarios

Article *in* Advances in Climate Change Research · September 2020

CITATION
1

READS
21

2 authors:

Jian Cao
Nanjing University of Information Science & Technology
32 PUBLICATIONS **391** CITATIONS
SEE PROFILE

Haikun Zhao
Nanjing University of Information Science & Technology
53 PUBLICATIONS **494** CITATIONS
SEE PROFILE

KeAi
CHINESE ROOTS
GLOBAL IMPACT

Available online at www.sciencedirect.com

ScienceDirect

Advances in Climate Change Research 11 (2020) 161−171

www.keaipublishing.com/en/journals/accr/

Distinct response of Northern Hemisphere land monsoon precipitation to transient and stablized warming scenarios

CAO Jian[a,b,*], ZHAO Hai-Kun[a]

[a] *Key Laboratory of Meteorological Disaster, Ministry of Education (KLME)/Joint International Research Laboratory of Climate and Environment Change (ILCEC)/Collaborative Innovation Center on Forecast and Evaluation of Meteorological Disasters (CIC-FEMD), Nanjing University of Information Science and Technology, Nanjing, 210044, China*

[b] *Earth System Modeling Center, Nanjing University of Information Science and Technology, Nanjing, 210044, China*

Received 18 March 2020; revised 15 May 2020; accepted 9 September 2020
Available online 16 September 2020

Abstract

To better understand the climate response under stabilized, overshoot, and transient global warming, four types of ensemble experiments on 1.5 °C/2 °C global warming scenarios (i.e., stabilized 1.5 °C, 1.5 °C overshoot, stabilized 2 °C, and transient 2 °C) are elaborately designed using the Nanjing University Information Science and Technology Earth System Model (NESM). Compared with the modern climate (1985−2014), the projected surface air temperature (SAT) change is characterized by a robust 'Northern Hemisphere (NH)-warmer than-Southern Hemisphere (SH)' and 'land-warmer than-ocean' patterns. The projected precipitation change exhibits 'NH-wetter than-SH' pattern in the tropics. Although the response of SAT and precipitation climatology show similar pattern between stabilized and overshoot scenarios, some significant differences are still found. The projected change in the Northern Hemisphere land monsoon precipitation (NHLMP) is 30% larger in the transient 2 °C experiment compared with that in the stabilized 2 °C experiment. The more vigorous NHLMP in the transient global warming scenario is mainly due to the enhanced land−sea thermal contrast and interhemispheric temperature difference. The enlarged land−sea thermal contrast increases the surface pressure gradient between the NH continents and its adjacent oceans, thus enhancing the NH monsoon circulation and moisture convergence. The enhanced interhemispheric temperature difference shifts the Hadley circulation and intertropical convergence zone northward, leading to the enhanced moisture convergence and the shifts of tropical rain band over the NH monsoon region. This result highlights that climate responses may depend on different warming trajectories and, which could facilitate the strategic planning of governments.

Keywords: 1.5 °C/2 °C global warming; Monsoon precipitation; NESM model; Transient global warming; Stabilized global warming

1. Introduction

The Northern Hemisphere land monsoon (NHLM) region is inhabited by ~60% of the world's population; however, the precipitation change in the NHLM region is less understood under the warming target of 1.5 °C/2 °C (IPCC, 2018). Understanding the driving mechanisms and reliable projection of NHLM precipitation (NHLMP) can benefit agriculture planning, food security, and socioeconomic sustainable development. Observational studies have shown a decline in NHLMP during the late 20th century and an enhancement afterward; this trend was mainly due to the external forcing of climate change and the internal variability of the earth system (Wang and Ding, 2006; Wang et al., 2012, 2013, 2017; Huang et al., 2019).

The NHLMP is projected to increase under RCP4.5 and RCP8.5 of CMIP5 (Kitoh et al., 2013; Hsu et al., 2013; Lee and Wang, 2014), and Shared Socioeconomic Pathway 2-4.5

* Corresponding author. Key Laboratory of Meteorological Disaster, Ministry of Education (KLME)/Joint International Research Laboratory of Climate and Environment Change (ILCEC)/Collaborative Innovation Center on Forecast and Evaluation of Meteorological Disasters (CIC-FEMD), Nanjing University of Information Science and Technology, Nanjing, 210044, China.
E-mail address: jianc@nuist.edu.cn (CAO J.).

Peer review under responsibility of National Climate Center (China Meteorological Administration).

https://doi.org/10.1016/j.accre.2020.09.007

(SSP2-4.5) of CMIP6 (Wang et al., 2020). Moisture budget analysis revealed that moisture convergence plays an essential role in the enhancement of monsoon precipitation (Hsu et al., 2013; Kitoh et al., 2013; Endo and Kitoh, 2014). The enhanced moisture convergence is due to the combination of two offset effects between the increased atmospheric moisture content due to the surface warming (thermodynamic effect) and weakened monsoon circulation because of greenhouse gas (GHG) induced top-heavy warming (dynamic effect) (Chadwick et al., 2013; Endo and Kitoh, 2014). Meanwhile, over the Northern Hemisphere (NH) monsoon regions, especially over the Asian monsoon region, the projected slowdown of monsoon circulation is smaller than other monsoon regions (Hsu et al., 2013; Endo and Kitoh, 2014). Lee and Wang (2014) and Wang et al., (2020) further argued that the projected increases in land−ocean and interhemispheric thermal contrasts, and an El Niño−like warming are all responsible for the differential changes of monsoon circulation between the NH and Southern Hemisphere (SH).

King et al. (2020) found that the land and NH surfaces are projected to be warmer in transient climate compared with that in quasi-equilibrium climate under the same magnitude of global warming. The land−ocean and NH−SH thermal contrasts could change global circulation, especially over the tropics (Lee and Wang, 2014; Park et al., 2015; Rowell and Chadwick, 2018; Cao et al., 2020). The difference in surface warming pattern and its associated circulation change may alter the NH monsoon precipitation. Cao et al. (2020) pointed out that the increasing of NH−SH thermal contrast tends to enhance the northward cross-equatorial flow and strengthen the boreal summer Hadley circulation, especially over the eastern Hemisphere. Such circulation change could further regulate the monsoon precipitation, especially over the NH monsoon region.

In the Paris Agreement, several global mean surface temperature (GMST) warming scenarios have been proposed under the targets of global warming 1.5 °C above preindustrial levels by the end of the 21st century (IPCC, 2018). These scenarios include the GMST passing through the threshold of 1.5 °C before the end of the 21st century, keeping at 1.5 °C during the late 21st century, and reaching an equilibrium state before 2100 and maintaining the temperature for centuries (IPCC, 2018). Therefore, assessing the impacts of 1.5 °C/2 °C global warming would enhance our understanding of possible responses for the transient, short-term (~3−5 decades) stabilized, and long-term equilibrium climate of the earth system (IPCC, 2018).

Giving the different responses in SAT among difference scenarios (e.g., Pendergrass et al., 2015; King et al., 2020), it is still unclear that how would the NHLMP change and what are the differences of monsoon precipitation response among different scenarios. Motivated by this, we designed four 1.5 °C/2 °C transient and stabilized global warming scenarios using the NESM3 to understand the driven mechanism of NHLMP change in difference warming scenarios. In addition, this study will also provide the dataset for accessing the climate impacts of 1.5 °C/2 °C global warming.

2. Experimental design and data

2.1. Model and experimental design

The NESM3 model is used to perform the ensemble simulations for different global warming scenarios, which consists of the atmospheric component model of ECHAM v6.3, the ocean component model of NEMO v3.4, the sea ice component model of CICE v4.1, and the OASIS3-MCT_3.0 coupler (Cao et al., 2018). The JSBACH land surface component model is implicitly coupled with the ECHAM model. The NESM3 model has two subversions, namely, the standard and lower resolution versions. In this study, the standard resolution version of the NESM3 model is configured; this version has the same configuration as theNESM3 CMIP6 experiment (Cao et al., 2019a). The atmospheric component model has a resolution of T63L47 (~1.9° latitude × 1.9° longitude) and 47 vertical levels extending from the surface to 0.01 hPa. The horizontal resolution of the ocean component model is ~1° in longitudinal and latitudinal directions, and the resolution in the meridional direction is refined to 1/3° over the tropical region. The ocean model has 46 vertical layers, with ten layers in the upmost 100 m. The horizontal resolution of the sea ice model is ~1 × 0.5° in longitudinal and latitudinal directions. The CICE v4.1 solves dynamic and thermodynamic equations for five categories of ice thickness. Detailed information on the description and development of the model can be found in Cao et al. (2018). The capability of NESM3 model in simulating modern climatology and climate modes are evaluated in Cao et al. (2015, 2018). This model is also used in understanding the predictability of global monsoon precipitation on decadal to multi-decadal time scale (Li et al., 2017; Wang et al., 2018), the monsoon precipitation response to different external forcing (Yan et al., 2018; Cao et al., 2019b, 2019c) and the predictability of extreme events (Luo and Wang, 2018; Wang et al., 2019).

To investigate the climate impacts of 1.5 °C/2 °C global warming, we elaborately design four global warming scenarios, e.g., stabilized 1.5 °C (15 ks), 1.5 °C overshoot (15 kos), stabilized 2 °C (2 ks), and transient 2 °C (2 kt). The reference period of the GMST is 1850−1899. For the stabilized 1.5 °C scenario, the GMST warming should be stabilized at the level of 1.5 °C (1.5 ± 0.1 °C) above preindustrial levels for at least three decades by 2100. The 1.5 °C overshoot scenario is similar to the stabilized 1.5 °C scenario except that the expected multiyear GMST slightly overshoots before returning to the global warming criterion of 1.5 °C by the end of the 21st century. The design of the stabilized 2 °C scenario is the same as the stabilized 1.5 °C scenario except that the warming criterion is 2 °C. The additional transient 2 °C scenario assumes that the expected GMST is continuously increasing in the 21st century. The result of the transient 2 °C scenario is used to assess the difference and similarity of climatic consequences under transient and stabilized global warming. A set of five ensembles of each scenario branching from the NESM3 CMIP6 preindustrial experiment is conducted.

The integration of the four groups of experiments spans from 1850 to 2100. The time-lag method is used to initialize the five realizations. During the historical period (1850−2014), all ensembles are driven by the CMIP6 historical experiment forcing, including greenhouse gas concentrations, global land use, and land-cover forcing dataset, solar irradiance, prescribed aerosol, and ozone concentration (Cao et al., 2019). During the period of 2015−2100, the differences in CO_2 concentrations are only considered among the four global warming scenarios. All other forcing take the same values in 2014. To fulfill the requirement of changes in GMST under the four designed scenarios, we conduct experiments on the basis of two aspects. First, we design the CO_2 concentration pathways on the basis of the Community Earth System Model results and scale it by the equilibrium climate sensitivity of the NESM3 model. Second, a few CO_2 concentration perturbation experiments are performed to obtain the final CO_2 concentration pathway for each global warming scenario. The identification of the equilibrium climate sensitivity is determined on the basis of the changes in the GMST in response to the doubling of CO_2 concentration from preindustrial levels. The CO_2 concentration pathways could vary in different coupled models due to the differences in equilibrium climate sensitivities.

2.2. Data and method

The 1985−2014 precipitation data of the Global Precipitation Climatology Project version 2.2 (Huffman et al., 2009) are used to define the monsoon domain. According to Wang et al. (2012), the monsoon region is defined as where the boreal summer (May−September) precipitation exceeds 55% of the total annual amount and the annual range of precipitation is larger than 2.5 mm d^{-1}. We also adopt the global monsoon domains derived from the historical (1985−2014) and stabilized 1.5 °C experiments (2071−2100) which yield similar results (not shown).

The period of 1985−2014 is taken as a reference period for modern climatology. To make a fairly comparison, the period of 2071−2100 is selected for the stabilized 1.5 °C and 1.5 °C overshoot scenario since that the GMST warming is 1.5 °C above pre-industrial levels. The periods of 2071−2100 and 2032−2061 are used for the stabilized and transient 2 °C scenario, respectively, due to the same magnitude (2 °C above pre-industrial levels) of global warming. The statistical significance of correlation and composite differences are performed using two-tailed Student's *t*-test (Siegel, 1956).

3. Results

3.1. Mean surface air temperature and precipitation

The temporal evolutions of CO_2 concentration in the four scenarios are shown in Fig. 1a. In the stabilized 1.5 °C scenario, the atmospheric CO_2 concentration gradually increases and reaches the maximum value of 450×10^{-6} in 2035. Then, the CO_2 concentration declines to 430×10^{-6} in 2055. Naturally, a net negative emission is expected after 2035. Observation data show that the CO_2 concentration is 413×10^{-6} at the beginning of 2020 and increases by approximately 20×10^{-6} in 2010s (Meinshausen and Elisabeth, 2016). This trend suggests that immediate action should be taken to pursue global warming under 1.5 °C. In the 1.5 °C overshoot scenario, the CO_2 concentration is projected to reach the maximum value of 490×10^{-6} in 2040. This scenario requires a more extensive negative CO_2 emission from 2041 to 2049. After that, the CO_2 concentration maintains a constant of 424×10^{-6} until 2100. Under the stabilized 2 °C scenario, the CO_2 concentration is projected to reach the maximum value of 500×10^{-6} in 2050 and then gradually to decay to 480×10^{-6} in 2075. Subsequently, the CO_2 emission is projected to be maintained at zero until 2100. For the transient 2 °C warming scenario, the CO_2 emission follows the CMIP6 SSP5-8.5 emission. It shows a rapid increasement of atmospheric CO_2 concentration.

We first verify the model's capability in simulating the designed temperature for different warming trajectories. In the stabilized 1.5 °C scenario (Fig. 1b), the GMST anomaly exceeding 1.5 °C above preindustrial level is projected to occur in 2049. Then, it would maintain the value till 2100, with a linear trend of 0.01 °C per decade during 2051−2100. Driven by the 1.5 °C overshoot CO_2 concentration pathway, the GMST warming is projected to exceed 1.5 °C in 2031 and then to reach its maximum of 1.9 °C in 2053. Afterward, the GMST gradually decreases to ~1.5 °C till 2100, with linear trend of −0.03 °C per decade in 2071−2100. In the stabilized 2 °C scenario, the GMST anomaly is projected to rise by 2 °C in 2050; this value would be sustained until 2100, with a linear trend of 0.02 °C per decade during 2050−2100. Under the transient 2 °C CO_2 forcing, the GMST is projected to continuously increase until 2100. Similar projection of GMST are projected in the five ensembles of each scenario, indicating a reasonable design of CO_2 concentration pathways (not shown). Furthermore, the GMST could exceed the warming criterion beyond 2100 in the stabilized scenarios due to the slow response of the ocean (Held et al., 2010).

Fig. 2 shows the changes of climatologic mean SAT with respect to modern climate and their differences among the four scenarios. Similar warming patterns are projected for the stabilized 1.5 °C and 1.5 °C overshoot experiments (Fig. 2a and c) and for the stabilized and transient 2 °C experiments (Fig. 2b and d). Generally, the projected SAT warming is larger in NH than that in the SH, and it is higher in high latitudes than that in low latitudes, especially over the NH. The land surface is found to be warmer than the ocean, and the NH ocean appears to be warmer than the Southern Ocean. However, the subpolar North Atlantic is found to be cooler than that of the modern climatologic mean. Such so-called Atlantic 'warming hole' is a common feature in observation and CMIP5 models under RCP4.5 (Rahmstorf et al., 2015; Menary and Wood, 2018). The decreased SAT is also projected over large part of the Southern Ocean, which is also observed in some CMIP5 models under the RCP4.5 scenario (IPCC, 2014). The temperature difference between the stabilized

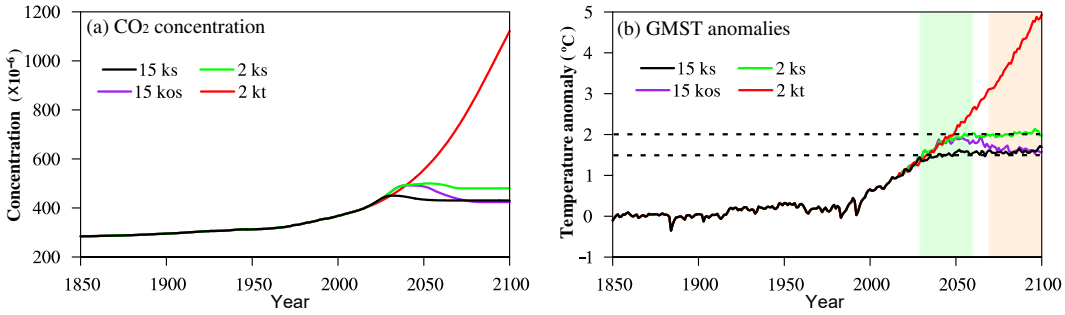

Fig. 1. Experimental design of 1.5 °C/2 °C global warming scenarios, (a) CO_2 concentration pathways in the stabilized 1.5 °C (15 ks), 1.5 °C overshot (15 kos), stabilized 2 °C (2 ks), and transient 2 °C (2 kt) global warming experiments; (b) ensemble means of GMST in the 15 ks, 15 kos, 2 ks, and 2 kt experiments. (The period for the stabilized 1.5 °C, 1.5 °C overshoot, and stabilized 2 °C experiments is 2071−2100 (yellow shade), and the period of 2032−2061 (green shade) is used for the transient 2 °C experiment. The dashed lines indicate the global warming of 1.5 °C/2 °C above preindustrial levels).

1.5 °C and 1.5 °C overshoot experiments is not significant and less than 0.1 °C over most of the globe (Fig. 2e). However, the difference between the stabilized and transient 2 °C experiments shows significantly warm anomalies over the mid−high latitudes of the NH and significantly cold anomalies over the mid−high latitudes of the SH (Fig. 2f).

The projected changes in precipitation are similar for all global warming scenarios (Fig. 3), showing a robust 'wet-get-wetter' pattern (Held and Soden, 2006). Significant increase is projected over the intertropical convergence zone (ITCZ) and the South Pacific convergence zone, as well as the midlatitude storm track regions where the moisture convergence and upward motion are generally strong. Over the equatorial region, precipitation is projected to decrease over the Indian Ocean and to increase over the western Pacific Ocean. This anomaly pattern is linked to the decreased sea surface temperature (SST) gradient across the equatorial Pacific and the associated weakened Walker circulation (not shown). The vertical motion is projected to decrease over the maritime continent but to enhance over the equatorial western Pacific region (not shown).

As shown in Fig. 3e, no significant difference is found between the stabilized 1.5 °C and 1.5 °C overshoot experiments. However, the North African monsoon is projected to be significantly wetter under the transient 2 °C experiment than that under the stabilized 2 °C experiment. Moreover, the southwestern Pacific Ocean is projected to be significantly drier under the transient 2 °C experiment than that under the stabilized 2 °C experiment, suggesting different precipitation responses under transient and stabilized global warming.

3.2. Land monsoon precipitation over the NH

Over the NH, monsoon precipitation accounts for a large portion of annual precipitation. Fig. 4 shows the changes in boreal summer precipitation for the four scenarios. Compared with the changes in annual precipitation, boreal summer precipitation over the tropics shifts northward and is mainly associated with the northward movement of the ITCZ (Fig. 4a–c, Wang et al., 2013). Over the NH land, the enhancement of summer precipitation is mainly projected to be located in the monsoon region, especially over the North African and Asian monsoon regions. The monsoon precipitation is increased by 0.6 mm d^{-1} over the North African and Indian monsoon region, while the projected North American is drier than modern climate state. This east-west asymmetric change of NH monsoon precipitation is also found in CMIP5/CMIP6 projection (Lee and Wang, 2014; Hsu et al., 2013). This asymmetric change is attributable to the GHG forcing because the only difference is GHG concentration in the four global warming experiments.

Fig. 4e shows that the difference of boreal summer NHLMP is little between stabilized 1.5 °C and 1.5 °C overshoot experiments. However, the projected difference is large between the transient 2 °C experiment and the stabilized 2 °C experiment (Fig. 4f). The enhancement of land monsoon precipitation is more pronounced over the North African monsoon region in the transient 2 °C experiment compared with that in the stabilized 2 °C experiment. The significant difference of land monsoon precipitation between the transient and stabilized global warming may suggest the dependence of hydrologic response on warming trajectory.

Fig. 5 shows the ensemble means of NHLMP anomalies, land−sea thermal contrast indices, and interhemispheric temperature difference indices in the four warming scenarios. The land−sea thermal contrast is defined as the difference of SAT over the NH continent and the global ocean (60°S−60°N, 180°W−180°E). The interhemispheric temperature difference is computed as the difference of SAT between 20° and 60°N, 180°W−180°E and 40°S−0°, 180°W−180°E. Here, the reference period is 1850−1899. The NHLMP decreased in the 1850s−1900s and 1950s−1990s and increased in the 1900s−1940s and after the 1990s (Fig. 5a). The simulated historical NHLMP variation since 1900 is consistent with the observation data (Huang et al., 2019). The simulated NHLMP anomalies are significantly correlated ($r \geq 0.85$, $p < 0.01$) with the changes of land−sea thermal contrast and interhemispheric temperature difference (Fig. 5). The close relationships suggest that the NHLMP is likely driven by the land−sea thermal contrast and the interhemispheric temperature difference in 1850−2100.

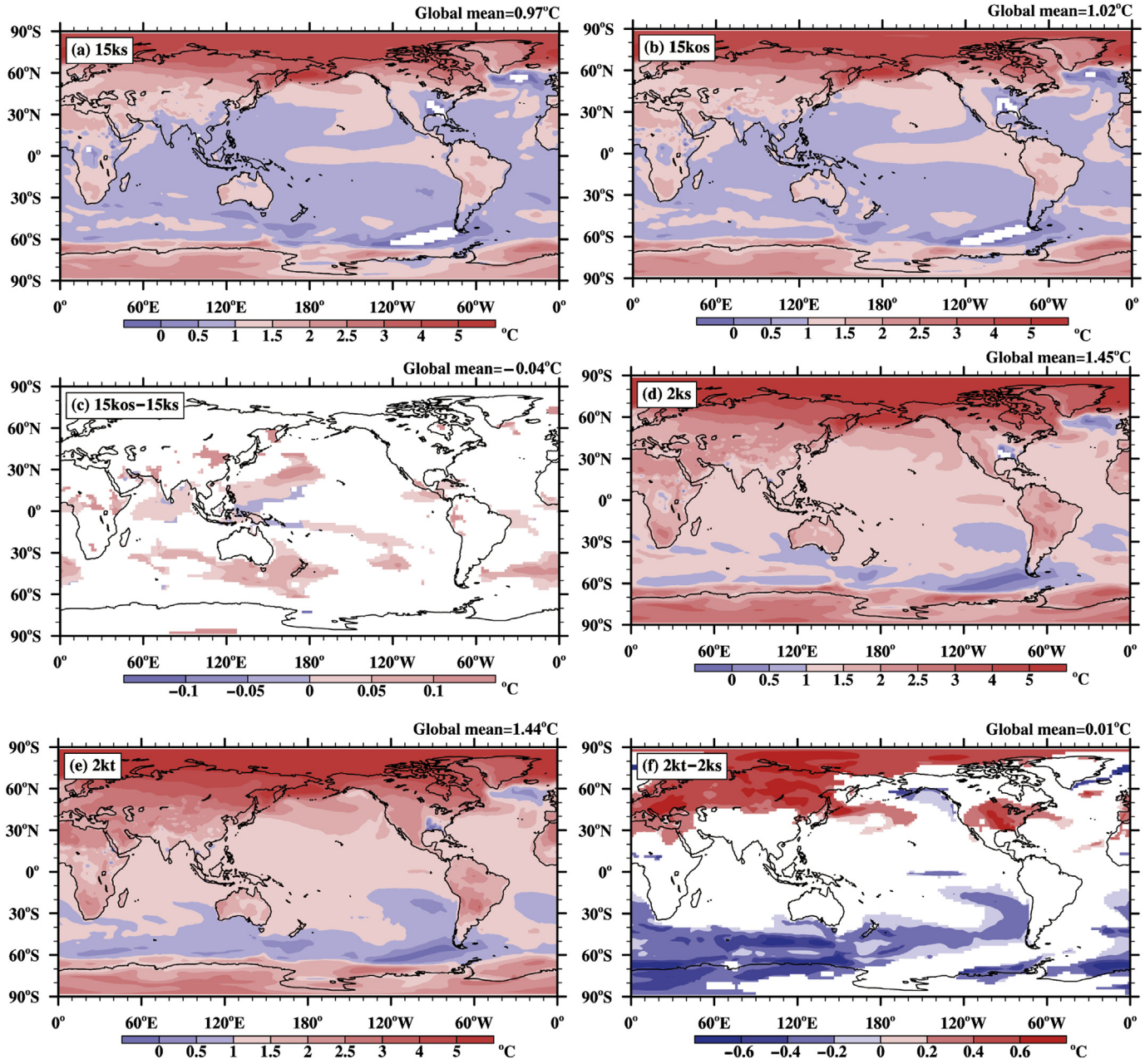

Fig. 2. Differences of SAT between the (a) stabilized 1.5 °C, (b) stabilized 2 °C, (c) 1.5 °C overshoot, (d) transient 2 °C scenario and modern climatology (1985−2014); differences of SAT (e) between the stabilized 1.5 °C and 1.5 °C overshoot experiments, and (f) between the stabilized and transient 2 °C experiments (Only values that are statistically significant at 95% confidence level are shown. The period for the stabilized 1.5 °C, 1.5 °C overshoot, and stabilized 2 °C experiments is 2071−2100, and the period of 2032−2061 is used for the transient 2 °C experiment).

We further calculate the NHLMP in the transient 2 °C experiment during 2032−2061 when the GMST rises 2 °C with respect to the preindustrial levels. The NHLMP is projected to increase by ~6% (0.43 mm d^{-1}) in the transient 2 °C experiment (2032−2061) compared with modern climatology. It is approximately 30% larger than that in the stabilized 2 °C experiment (2071−2100). The difference in precipitation between the stabilized and transient warming is larger than that of an additional stabilized 0.5 °C warming (stabilized 1.5 °C vs. stabilized 2 °C). In the transient 2 °C experiment, the land−sea thermal contrast (interhemispheric temperature difference) is 0.25 °C (0.3 °C) larger than that in the stabilized 2 °C experiment (2071−2100). The larger land−sea thermal contrast could deepen the continental low-pressure system and strengthen the ocean high-pressure system during the boreal summer, leading to a larger surface pressure gradient between land and ocean (Webster, 1987; Fasullo, 2012). Fig. 6a shows the difference of surface pressure between the transient and stabilized 2 °C experiment. The surface pressure is projected to lower over

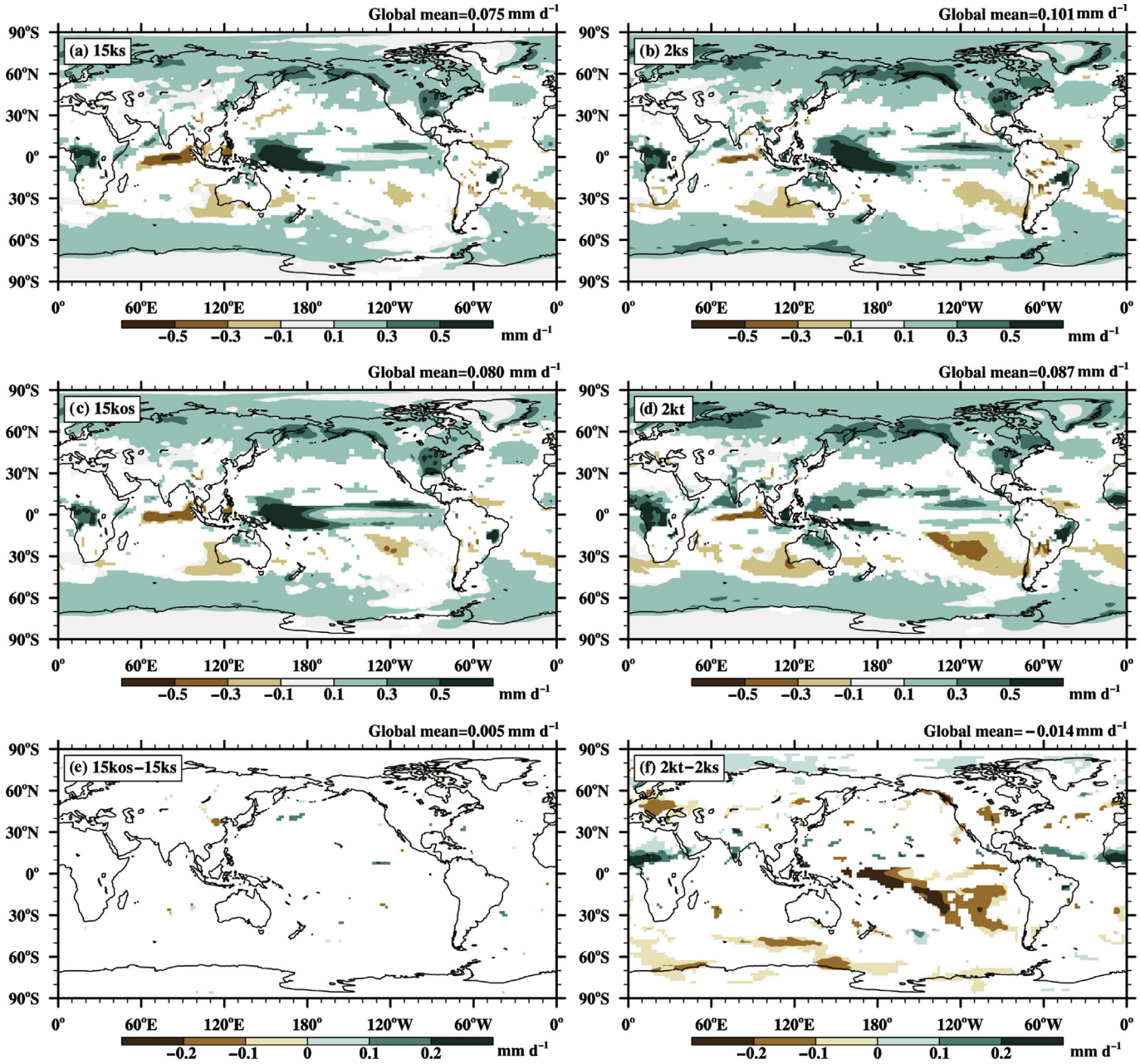

Fig. 3. Changes of annual precipitation between the (a) stabilized 1.5 °C, (b) stabilized 2 °C, (c) 1.5 °C overshoot, (d) transient 2 °C scenario and modern climatology (1985−2014); difference of precipitation (e) between the stabilized 1.5 °C and 1.5 °C overshoot experiments and (f) between the stabilized and transient 2 °C experiments (Only values that are statistically significant at 95% confidence level are shown. The period for the stabilized 1.5 °C, 1.5 °C overshoot, and stabilized 2 °C experiments is 2071−2100, and the period of 2032−2061 is used for the transient 2 °C experiment).

the mid−high latitudes of the NH continents and higher over the tropical oceans under transient global warming. The enhanced surface pressure gradients between the NH continents and its adjacent ocean could drive the boreal summer low-level monsoon flow (Fig. 6a, Webster, 1987). Compared with the stabilized 2 °C experiment, the transient 2 °C experiment simulates more robust cross-equatorial flow over the Indian Ocean, western Pacific Ocean, and Atlantic Ocean. And the southwesterly monsoon flow brings more moisture that transports into the NH land monsoon region, leading to the enhancement of low-level moisture convergence over the NH monsoon regions (Figs. 6a and 7b).

During the boreal summer, the climatological mean upward branch of Hadley circulation is located over the NH tropics (Fig. 6b). In the transient 2 °C experiment, the projected ascent motion is stronger (weaker) than the stabilized 2 °C experiment over the region north (south) of 8°N (Fig. 6b). The stronger ascent motion is consistent with the more vigorous moisture convergence over the NH monsoon region, thus leads to more monsoon precipitation in the transient 2 °C experiment. Besides, the transient 2 °C experiment projected a stronger ascent motion over the region of 10°−30°N, leading to a northward expanding of upward branch of Hadley circulation over the NH (Fig. 6b).

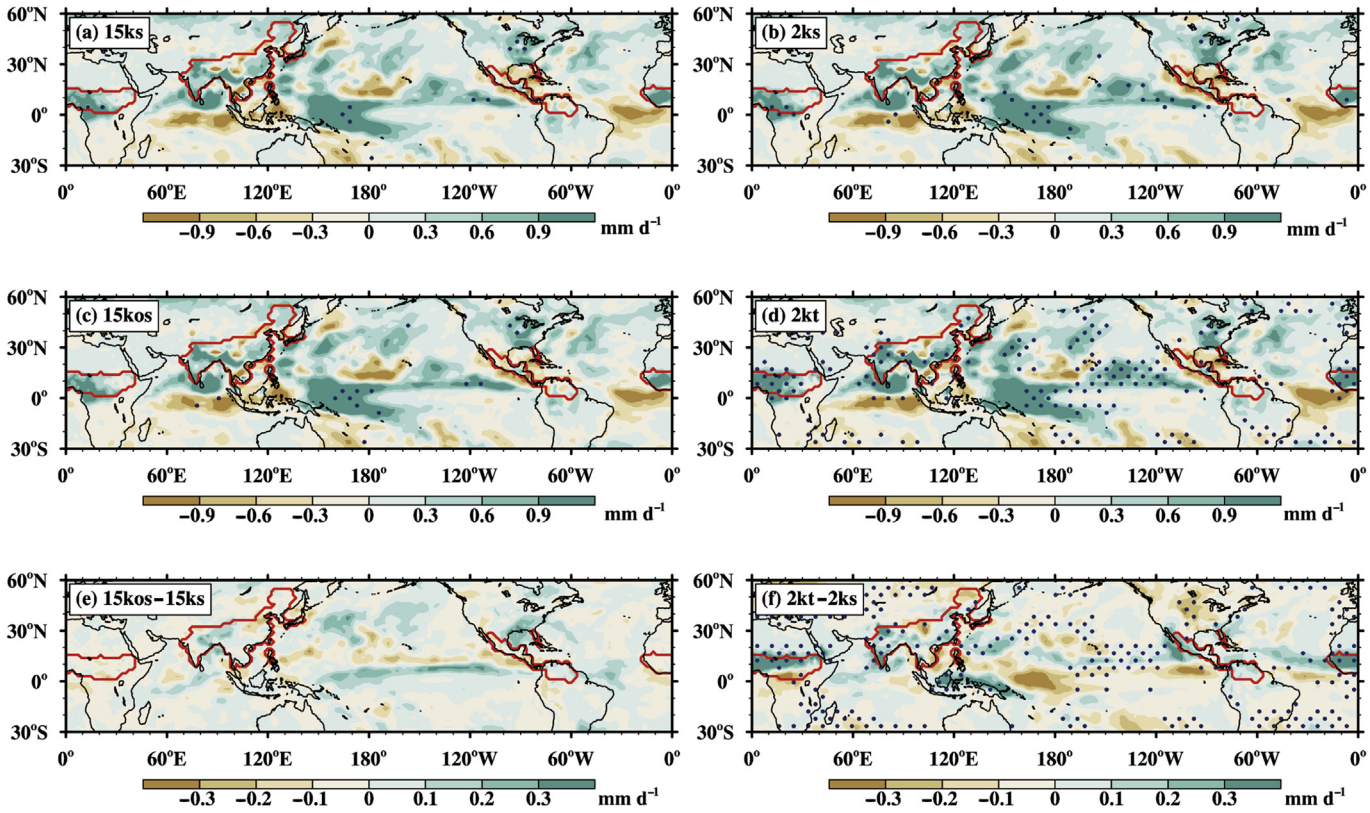

Fig. 4. Changes of boreal summer (May−September) precipitation between the (a) stabilized 1.5 °C, (b) stabilized 2 °C, (c) 1.5 °C overshoot, and (e) transient 2 °C scenarios and modern climatology (1985−2014); difference of boreal summer precipitation (c) between the stabilized 1.5 °C and 1.5 °C overshoot experiments, and (f) between the stabilized and transient 2 °C experiments (Stippling indicates statistically significant at 95% confidence level. The red lines outline the NH land monsoon region. The period for the stabilized 1.5 °C, 1.5 °C overshoot, and stabilized 2 °C experiments is 2071−2100, and the period of 2032−2061 is used for the transient 2 °C experiment).

Previous studies pointed out the shift of Hadley circulation is closely linked to the movement of ITCZ which is driving by the atmospheric cross-equatorial heat transport (Donohoe et al., 2013; Schneider et al., 2014; Xiang et al., 2018). The cross-equatorial energy transport could cause by interhemispheric SST difference over both tropical and extratropical region. Compared with the stabilized 2 °C experiment, the transient 2 °C experiment simulates significantly warmer NH oceans and a cooler Southern Ocean (Fig. 7b). Such warming and cooling of the oceans increase the interhemispheric thermal contrast, resulting in the northward shifting of the ITCZ and Hadley circulation by enhancing the cross-equatorial heat transport (Fig. 6b). Therefore, ITCZ-associated precipitation is enhanced over the NH monsoon region. Cao et al. (2020) also pointed out a model with larger interhemispheric temperature difference tends to enhance NH monsoon precipitation by shifting the ITCZ and Hadley circulation positions.

We also compare the simulated NHLMP in the stabilized 1.5 °C and 1.5 °C overshoot experiments. Precipitation is comparable with each other under these two scenarios. Moreover, the simulated SST and low-level circulation have no significant difference over most of globe under the stabilized and overshoot scenario (Fig. 7a).

In summary, the simulated NHLMP is more vigorous under transient 2 °C global warming compared with that under stabilized 2 °C global warming, but there is no significant difference in projected precipitation between stabilized 1.5 °C and 1.5 °C overshoot experiments. The vigorous monsoon precipitation is caused by the enlarged land−sea thermal contrast and interhemispheric temperature difference. The former increases the surface pressure gradient between NH continental and its adjacent ocean, leading to strengthening of monsoon circulation. The latter can shift the ITCZ and Hadley circulation northward resulting in the northward shift of rain band. Both mechanisms are benefit to the enhancement of NHLMP.

4. Discussion and conclusion

Four CO_2 concentration pathways were elaborately designed with the NESM3 model to produce the 1.5 °C/2 °C global warming scenarios (including stabilized 1.5 °C, 1.5 °C overshoot, stabilized, and transient 2 °C experiments). We integrated five ensembles for each of the four scenarios. These simulations produced the evolutions of GMST as expected, thus raising our confidence in assessing the climate impacts of the 1.5 °C/2 °C global warming.

Under 1.5 °C/2 °C global warming scenario, the changes of the climatologic mean of SAT are all characterized by a warmer NH than SH, a warmer land surface than ocean, and a warmer higher latitude than lower latitudes patterns.

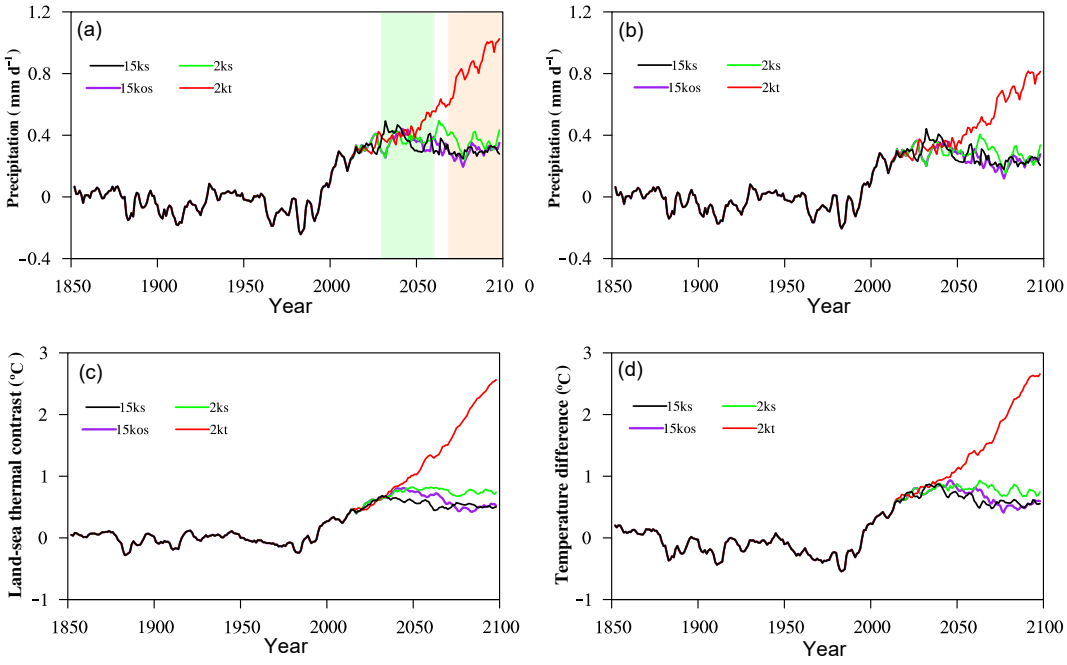

Fig. 5. Multi-ensemble means of boreal summer Northern Hemisphere land monsoon precipitation anomalies in the stabilized 1.5 °C (15 ks), 1.5 °C overshot (15 kos), stabilized 2 °C (2 ks), and transient 2 °C (2 kt) global warming experiments (a); (b) same as (a) except that the boreal summer global averaged precipitation trend is removed; (c) land−sea thermal contrast indices; (d) interhemispheric temperature differences. The land−sea thermal contrast is defined as the difference of SAT over the NH continent and the global ocean (60°S−60°N, 180°W−180°E). The interhemispheric temperature difference is computed as the difference of SAT between 20°N and 60°N, 180°W−180°E and 40°S−0°, 180°W−180°E. The reference period is 1850−1899. The period for the stabilized 1.5 °C, 1.5 °C overshoot, and stabilized 2 °C experiments is 2071−2100 (yellow shade), and the period of 2032−2061 (green shade) is used for the transient 2 °C experiment. The dashed lines indicate the global warming of 1.5 °C/2 °C above preindustrial levels).

Moreover, the changes of precipitation are all featured by 'NH-wetter than-SH' pattern in the tropics and wetter high−latitude storm track regions. The climatologic mean temperature and precipitation are similar between stabilized 1.5 °C and 1.5 °C overshoot experiments. However, the climate responses (including temperature, precipitation, and circulation) are significantly different between transient and stabilized 2 °C global warming, especially over the NH monsoon region.

The response of monsoon precipitation to transient global warming has been extensively explored in previous studies (Hsu et al., 2013; Kitoh et al., 2013; Lee and Wang, 2014), while it is less compared with the response to stabilized or overshoot scenario. Under the transient global warming, the projections from CMIP5/6 experiments indicated an increasement of NHLMP due to the enhanced moisture flux convergence over the monsoon regions (Kitoh et al., 2013; Wang et al., 2020). This convergence is dominated by the moistening of atmospheric although it is partially offset by the weakening of tropical circulation (Hsu et al., 2013; Kitoh et al., 2013; Wang et al., 2020). This thermodynamic argument is challenged by the dynamic argument that the change of monsoon precipitation is the results of tropical circulation shifting, since the effect of enhancement of moisture is canceled by the weakening of mean tropical circulation. Under the transient global warming, the projected SAT warming shows the 'NH-warmer than-SH' and 'land-warmer than-ocean' patterns (Fig. 2; Wang et al., 2020). King et al. (2020) revealed the two SAT warming patterns are more prominent under transient global warming compare to stabilized warming under the same magnitude of global warming. The two differential warming patterns are found to be important factors in explaining the NHLMP difference between the transient and stabilized global warming in this study.

The NHLMP is projected to be 30% greater for the transient 2 °C experiment than that for the stabilized 2 °C experiment. Such a phenomenon is mainly due to dynamic effect (circulation change) of the enlarged land−sea thermal contrast and interhemispheric temperature difference under the transient global warming. On one hand, the enlarged land−sea thermal contrast increases the surface pressure gradients between the NH continents and its adjacent ocean, thus enhancing the NH monsoon circulation. Moreover, it transports more moisture to the monsoon region; therefore, the monsoon precipitation is enhanced. In addition, the strengthened moisture convergence enhances the Hadley circulation that also reinforces the NH monsoon precipitation. On the other hand, under the transient 2 °C warming, the projected boreal summer ascent branch of Hadley circulation is stronger (weaker) than the stabilized 2 °C warming over the region north (south) of 8°N. This is associated with the more northward expansion of Hadley circulation in the transient 2 °C experiment. It is known that the shift of Hadley circulation is coincident with the movement of ITCZ, which is commonly driving by the interhemispheric differential warming-induced cross-equatorial heat transport (Donohoe et al., 2013;

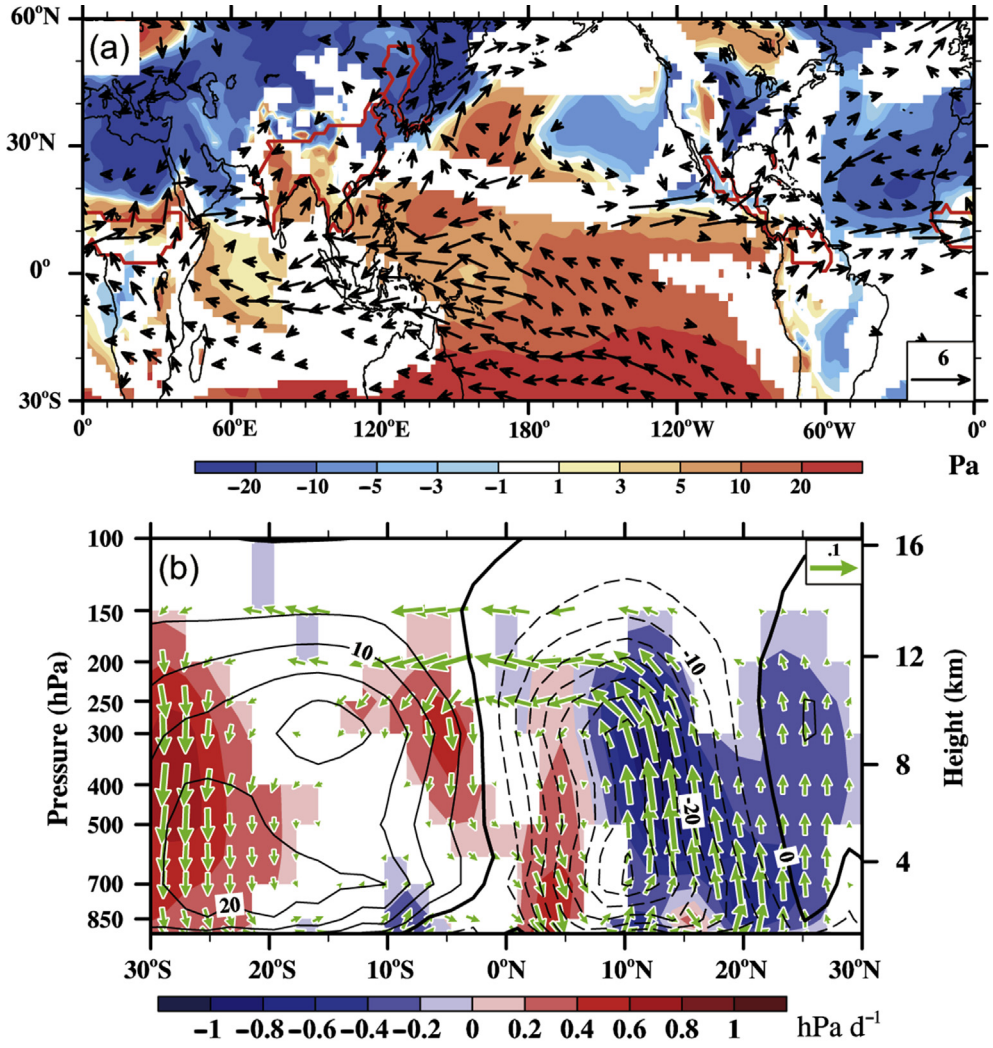

Fig. 6. Differences of (a) surface pressure and 850 hPa moisture flux (g kg^{-1} m s^{-1}), and (b) Hadley circulation between the transient (2071−2100) and stabilized 2 °C (2032−2061) global warming experiments (Contours in (b) represent the zonal mean vertical motion (ω, hPa d^{-1}) in the stabilized 2 °C experiment. Shading indicates the difference in vertical motion (ω, hPa d^{-1}). Vectors are the composite of vertical motions ($\omega \times 100$) and meridional winds (m s^{-1}). A negative/positive value of ω means ascent/decent motion. Only values that are statistically significant at 95% confidence level are shown).

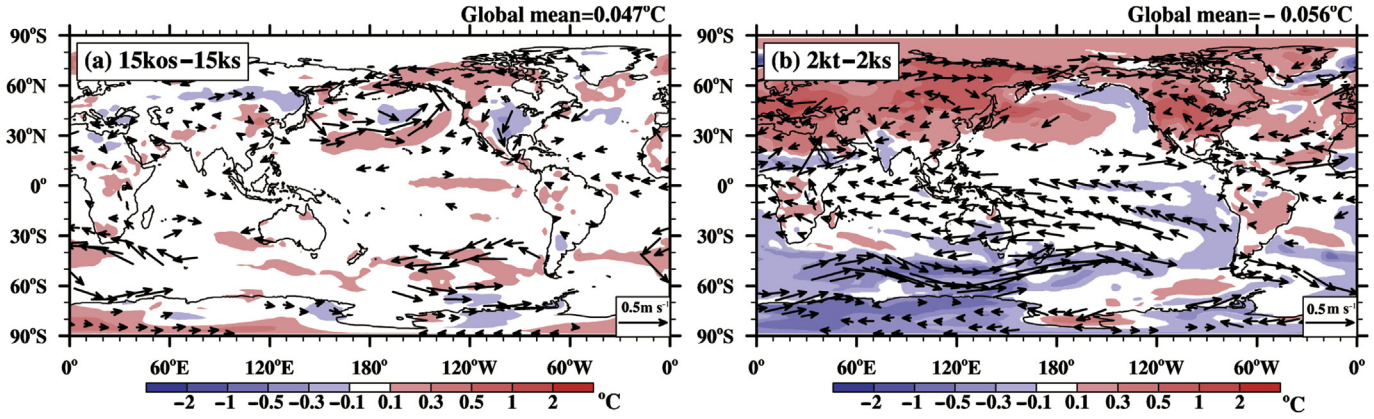

Fig. 7. Difference of surface temperature (shading) and 850 hPa wind (vector, m s^{-1}) (a) between the stabilized 1.5 °C (2071−2100) and 1.5 °C overshoot (2071−2100) experiments, and (b) between the stabilized (2071−2100) and transient 2 °C (2032−2061) experiments (Wind vectors are statistically significant at 95% confidence level by the Student *t* test).

Schneider et al., 2014; Xiang et al., 2018). Therefore, the vigorous NHLMP is produced when the ITCZ shift more northward in the transient 2 °C experiment.

In summary, this study suggests that the global impact largely depends on the different warming trajectories. Reducing the future GHG emission would benefit for reducing the risk of flooding summer over the NH monsoon region.

Declaration of competing interest

The authors declare no conflict of interest.

Acknowledgment

This work was supported by the National Key R & D Program of China (2017YFA0603801), the Natural Science Foundation of China of Jiangsu Province (BK20180812, BK20181412), and the Natural Science Foundation of China (42005017, 41922033).

References

Cao, J., Wang, B., Xiang, B., et al., 2015. Major modes of short-term climate variability in the newly developed NUIST Earth System Model (NESM). Adv. Atmos. Sci. 32, 585−600. https://doi.org/10.1007/s00376-014-4200-6, 2015.

Cao, J., Wang, B., Yang, Y., et al., 2018. The NUIST Earth System Model version 3: description and preliminary evaluation. Geosci. Model Dev. 11, 2975−2993.

Cao, J., Ma, L., Li, J., et al., 2019a. Introduction of NUIST-ESM model and its CMIP6 activities. Clim. Change Res. 15 (5), 566−570 (in Chinese).

Cao, J., Wang, B., Liu, J., 2019b. Attribution of the last glacial maximum climate formation. Clim. Dynam. 53, 1661−1679. https://doi.org/10.1007/S00382-019-04711-6.

Cao, J., Wang, B., Ma, L., 2019c. Attribution of global monsoon response to last glacial maximum forcings. J. Clim. 32, 6589−6605.

Cao, J., Wang, B., Wang, B., et al., 2020. Sources of the inter-model spread in projected global monsoon hydrologic sensitivity. Geophys. Res. Lett. https://doi.org/10.1029/2020GL089560.

Chadwick, R., Boutle, I., Martin, G., 2013. Spatial patterns of precipitation change in CMIP5: why the rich do not get richer in the tropics. J. Clim. 26, 3803−3822. https://doi.org/10.1175/JCLI-D-12-00543.1.

Donohoe, A., Marshall, J., Ferreira, D., et al., 2013. The relationship between ITCZ location and cross-equatorial atmospheric heat transport: from the seasonal cycle to the last glacial maximum. J. Clim. 26 (11), 3597−3618. https://doi.org/10.1175/JCLI-D-12-00467.1.

Endo, H., Kitoh, A., 2014. Thermodynamic and dynamic effects on regional monsoon rainfall changes in a warmer climate. Geophys. Res. Lett. 41, 1704−1710. https://doi.org/10.1002/2013GL059158.

Fasullo, J., 2012. A mechanism for land−ocean contrasts in global monsoon trends in a warming climate. Clim. Dynam. 39, 1137−1147.

Held, I., Soden, B., 2006. Robust responses of the hydrologic cycle to global warming. J. Clim. 19, 5686−5699.

Held, I., Winton, M., Takahashi, K., et al., 2010. Probing the fast and slow components of global warming by returning abruptly to preindustrial forcing. J. Clim. 23, 2418−2427.

Hsu, P., Li, T., Murakami, H., et al., 2013. Future change of the global monsoon revealed from 19 CMIP5 models. J. Geophys. Res. Atmos. 118 (3), 1247−1260. https://doi.org/10.1002/jgrd.50145.

Huffman, G., Adler, R., Bolvin, D., et al., 2009. Improving the global precipitation record: GPCP Version 2.1. Geophys. Res. Lett. 36, L17808.

Huang, X., Zhou, T., Zhang, W., et al., 2019. Northern Hemisphere land monsoon precipitation changes in the twentieth century revealed by multiple reanalysis datasets. Clim. Dynam. https://doi.org/10.1007/s00382-019-04982-z.

IPCC, 2014. Climate Change 2014: Impacts, Adaptation, and Vulnerability. Part A: Global and Sectoral Aspects. Contribution of Working Group II to the Fifth Assessment Report of the Intergovernmental Panel on Climate Change. Cambridge University Press, Cambridge and New York.

IPCC, 2018. An IPCC special report on the impacts of global warming of 1.5 °C above pre-industrial levels and related global greenhouse gas emission pathways, in the context of strengthening the global response to the threat of climate change, sustainable development, and efforts to eradicate poverty. https://www.ipcc.ch/sr15/download/#full.

King, A., Lane, T., Henley, B., et al., 2020. Global and regional impacts differ between transient and equilibrium warmer worlds. Nat. Clim. Change 10, 42−47. https://doi.org/10.1038/s41558-019-0658-7.

Kitoh, A., Endo, H., Krishna Kumar, K., et al., 2013. Monsoons in a changing world: a regional perspective in a global context. J. Geophys. Res. Atmos. 118, 3053−3065. https://doi.org/10.1002/jgrd.50258.

Lee, J., Wang, B., 2014. Future change of global monsoon in the CMIP5. Clim. Dynam. 42 (1−2), 101−119. https://doi.org/10.1007/s00382-012-1564-0.

Li, J., Wang, B., Yang, Y.M., 2017. Retrospective seasonal prediction of summer monsoon rainfall over West Central and Peninsular India in the past 142 years. Clim. Dynam. 48, 2581−2596.

Luo, X., Wang, B., 2018. Predictability and prediction of the total number of winter extremely cold days over China. Clim. Dynam. 50, 1769−1784.

Meinshausen, M., Elisabeth, V., 2016. Input4MIPs.CMIP6.CMIP.UoM.UoM-CMIP-1-2-0. Version on 20200805. Earth System Grid Federation. https://doi.org/10.22033/ESGF/input4MIPs.1118.

Menary, M., Wood, R., 2018. An anatomy of the projected North Atlantic warming hole in CMIP5 models. Clim. Dynam. 50, 3063−3080.

Park, J., Bader, J., Matei, D., 2015. Northern-Hemispheric differential warming is the key to understanding the discrepancies in the projected Sahel rainfall. Nat. Commun. 6, 5985.

Pendergrass, A., Lehner, F., Sanderson, B., et al., 2015. Does extreme precipitation intensity depend on the emissions scenario? Geophys. Res. Lett. 42 (20), 8767−8774.

Rahmstorf, S., Feulner, G., Mann, M., et al., 2015. Exceptional twentieth-century slowdown in Atlantic Ocean overturning circulation. Nat. Clim. Change 5, 475−480.

Rowell, D., Chadwick, R., 2018. Causes of the uncertainty in projections of tropical terrestrial rainfall change: East Africa. J. Clim. https://doi.org/10.1175/JCLI-D-17-0830.1.

Siegel, S., 1956. Nonparametric Statistics for the Behavioral Sciences. McGraw-Hill, New York.

Schneider, T., Bischoff, T., Haug, G., 2014. Migrations and dynamics of the intertropical convergence zone. Nature 513 (7516), 45−53. https://doi.org/10.1038/nature13636.

Wang, B., Ding, Q., 2006. Changes in global monsoon precipitation over the past 56 years. Geophys. Res. Lett. 33 (6), 1−4. https://doi.org/10.1029/2005GL025347.

Wang, B., Ji, C., Liu, J., 2020. Understanding future change of global monsoon projected by CMIP6 models. J. Clim. 33, 6471−6489.

Wang, B., Liu, J., Kim, H., et al., 2012. Recent change of the global monsoon precipitation (1979-2008). Clim. Dynam. 39 (5), 1123−1135. https://doi.org/10.1007/s00382-011-1266-z.

Wang, B., Liu, J., Kim, H., et al., 2013. Northern Hemisphere summer monsoon intensified by mega-El Niño/Southern oscillation and Atlantic multidecadal oscillation. PNAS 110 (14), 5347−5352. https://doi.org/10.1073/pnas.1219405110.

Wang, B., Li, J., Cane, M.A., et al., 2018. Toward predicting changes in land monsoon rainfall a decade in advance. J. Clim. 31, 2699−2714. https://doi.org/10.1175/JCLI-D-17-0521.1.

Wang, C., Wang, B., Cao, J., 2019. Unprecedented Northern Hemisphere tropical cyclone genesis in 2018 shaped by subtropical warming in the North Pacific and the North Atlantic. Geophys. Res. Lett. 46 (22), 13327−13337.

Wang, P., Wang, B., Cheng, H., et al., 2017. The global monsoon across time scales: mechanisms and out-standing issues. Earth Sci. Rev. 174, 84−121.

Webster, P., 1987. The elementary monsoon. In: Fein, J.S., Stephens, P.L. (Eds.), Monsoons. John Wiley, New York, pp. 3−32.

Xiang, B., Zhao, M., Ming, Y., et al., 2018. Contrasting impacts of radiative forcing in the Southern Ocean versus Southern Tropics on ITCZ position and energy transport in one GFDL climate model. J. Clim. 31, 5609−5628. https://doi.org/10.1175/JCLI-D-17-0566.1.

Yan, M., Wang, B., Liu, J., et al., 2018. Understanding the Australian monsoon change during the last glacial maximum with multi-model ensemble. Clim. Past 14, 2037−2052. https://doi.org/10.5194/cp-14-2037-2018.